Highly Efficient IR to NIR Upconversion in Gd2O2S: Er3+ for Photovoltaic Applications

ARTICLE *in* CHEMISTRY OF MATERIALS · MAY 2013

Impact Factor: 8.35 · DOI: 10.1021/cm4005745

8 AUTHORS, INCLUDING:

Stefan Fischer
University of California, Berkeley
46 PUBLICATIONS **450** CITATIONS
SEE PROFILE

Jan Christoph Goldschmidt
Fraunhofer Institute for Solar Energy Systems …
118 PUBLICATIONS **1,022** CITATIONS
SEE PROFILE

Bryce Sydney Richards
Karlsruhe Institute of Technology
166 PUBLICATIONS **3,794** CITATIONS
SEE PROFILE

Andries Meijerink
Utrecht University
364 PUBLICATIONS **13,529** CITATIONS
SEE PROFILE

CHEMISTRY OF MATERIALS

Article

pubs.acs.org/cm

Highly Efficient IR to NIR Upconversion in Gd_2O_2S: Er^{3+} for Photovoltaic Applications

Rosa Martín-Rodríguez,*[,†] Stefan Fischer,[‡] Aruna Ivaturi,[§] Benjamin Froehlich,[‡] Karl W. Krämer,[∥] Jan C. Goldschmidt,[‡] Bryce S. Richards,[§] and Andries Meijerink*[,†]

[†]Debye Institute for Nanomaterials Science, Department of Chemistry, Utrecht University, Princetonplein 5, 3584 CC Utrecht, The Netherlands

[‡]Fraunhofer Institute for Solar Energy Systems, Heidenhofstrasse 2, 79110 Freiburg, Germany

[§]Institute of Photonics and Quantum Sciences, School of Engineering and Physical Sciences, Heriot-Watt University, EH14 4AS Edinburgh, United Kingdom

[∥]Department of Chemistry and Biochemistry, University of Bern, Freiestrasse 3, 3012 Bern, Switzerland

ABSTRACT: Upconversion (UC) is a promising option to enhance the efficiency of solar cells by conversion of sub-bandgap infrared photons to higher energy photons that can be utilized by the solar cell. The UC quantum yield is a key parameter for a successful application. Here the UC luminescence properties of Er^{3+}-doped Gd_2O_2S are investigated by means of luminescence spectroscopy, quantum yield measurements, and excited state dynamics experiments. Excitation into the maximum of the $^4I_{15/2} \rightarrow {}^4I_{13/2}$ Er^{3+} absorption band around 1500 nm induces very efficient UC emission from different Er^{3+} excited states with energies above the silicon bandgap, in particular, the emission originating from the $^4I_{11/2}$ state around 1000 nm. Concentration dependent studies reveal that the highest UC quantum yield is realized for a 10% Er^{3+}-doping concentration. The UC luminescence is compared to the well-known Er^{3+}-doped β-$NaYF_4$ UC material for which the highest UC quantum yield has been reported for 25% Er^{3+}. The UC internal quantum yields were measured in this work for Gd_2O_2S: 10%Er^{3+} and β-$NaYF_4$: 25%Er^{3+} to be 12 ± 1% and 8.9 ± 0.7%, respectively, under monochromatic excitation around 1500 nm at a power of 700 W/m^2. The UC quantum yield reported here for Gd_2O_2S: 10%Er^{3+} is the highest value achieved so far under monochromatic excitation into the $^4I_{13/2}$ Er^{3+} level. Power dependence and lifetime measurements were performed to understand the mechanisms responsible for the efficient UC luminescence. We show that the main process yielding $^4I_{11/2}$ UC emission is energy transfer UC.

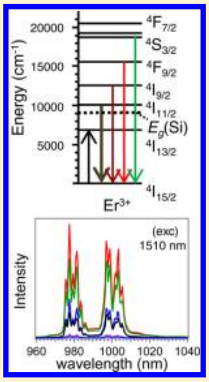

KEYWORDS: *upconversion, luminescence, quantum yield, solar cells*

INTRODUCTION

Upconversion (UC) processes, in which high energy photons are generated upon excitation with low energy photons, have attracted considerable attention since their discovery in the 1960s. Initially, the focus was on UC-materials for infrared (IR) detectors and UC lasers, but recently, new advanced applications have emerged, such as biolabeling and bioimaging, drug delivery, 3D-displays, and efficiency improvement of solar cells.[1−3] For solar cells (photovoltaics), an UC layer mounted beneath a bifacial solar cell can utilize the sub-bandgap photons. By UC of these photons to higher energy photons an increase of the maximum theoretical efficiency from ∼33% up to ∼40% is possible for a crystalline silicon (c-Si) solar cell (bandgap E_g = 1.1 eV, 1100 nm), if the UC process has maximum quantum yield.[3,4] Rare earth (RE)-doped systems are very suitable as UC materials because of their characteristic energy level structure and the limited vibrational losses related to the zero Stokes shift for $4f^n \rightarrow 4f^n$ transitions. The work presented in this paper involves the development of UC materials to increase the efficiency of c-Si solar cells.

Contrary to near-infrared (NIR) to visible (VIS) UC, studies of IR to NIR UC emission are limited although UC of wavelengths in the 1100−1700 nm region is very interesting for the potential harvesting of IR sunlight via c-Si solar cells. Recently, several studies have appeared and demonstrated proof of principle experiments for the enhancement of the efficiency of c-Si solar cells.[5,6] The studies show that Er^{3+} is a very promising ion for IR to NIR UC under excitation in the $^4I_{15/2} \rightarrow {}^4I_{13/2}$ absorption around 1500 nm, because the observed Er^{3+} UC emissions are within the c-Si absorption range. Different host materials have been compared in the literature. Initial experiments were performed using hexagonal sodium yttrium fluoride β-$NaYF_4$: Er^{3+}. The $NaYF_4$ host is well-known to yield efficient NIR to VIS UC when codoped with Yb^{3+} and Er^{3+}.[7] The singly Er^{3+}-doped material was shown to be very efficient for IR to NIR UC.[5,6] Also chloride lattices such as $BaCl_2$: Er^{3+} or pure $ErCl_3$ were found to show intense UC emission.[8,9] The IR to NIR UC luminescence has also been observed in both diluted $Cs_3Lu_2X_9$: 1%Er^{3+} and concentrated $Cs_3Er_2X_9$ systems (X = Cl, Br, I) for pulsed and continuous

Received: February 19, 2013
Revised: April 4, 2013
Published: April 5, 2013

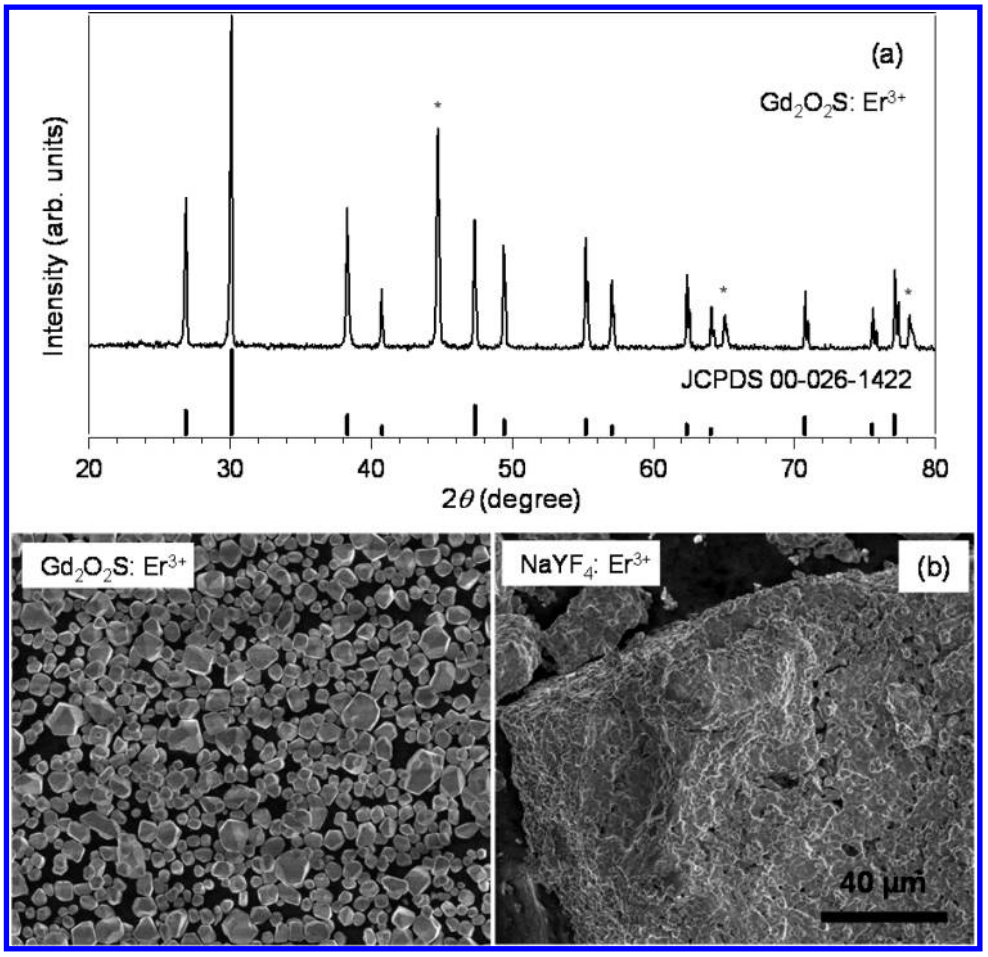

Figure 1. (a) XRD pattern measured for the Gd_2O_2S: 10%Er^{3+} sample, and peak positions of the hexagonal phase of Gd_2O_2S (JCPDS card no. 00-026-1422). * indicate peaks corresponding to the Al substrate. (b) SEM micrographs of Gd_2O_2S: 10%Er^{3+} (left) and $NaYF_4$: 25%Er^{3+} (right) microcrystalline samples (same scale bar in both images).

laser excitation at 1540 nm.[10] UC emission was also reported in CaF_2: Er^{3+}.[11] For $LiYF_4$: Er^{3+} the UC quantum yield was measured to be about 1.2% under high power excitation of 1.5 × 10^6 W/m^2.[12] Recently, Kumar et al. compared the UC luminescence properties of different oxysulfide phosphors M_2O_2S (M = Y, Gd, La) doped with 10%Er^{3+}, and concluded that of the three hosts, Gd_2O_2S: Er^{3+} is the most efficient sample for UC upon excitation into the $^4I_{13/2}$ level.[13]

β-$NaYF_4$ codoped with Er^{3+} and Yb^{3+} is the most efficient UC material showing VIS (green and red) emission upon NIR excitation, resonant with both $^4I_{15/2} \rightarrow {}^4I_{11/2}$ Er^{3+} and $^2F_{7/2} \rightarrow {}^2F_{5/2}$ Yb^{3+} transitions.[14,15] The origin of the intense VIS UC luminescence has been attributed to the low phonon energies and the disorder in the structure which gives multiple sites for Er^{3+} with slightly different energy level schemes. This has been proposed to give rise to additional resonance between Er^{3+} neighbors, resulting in efficient energy transfer leading to UC.[16] It is generally assumed that Er^{3+}-doped β-$NaYF_4$ UC phosphors are also the most efficient IR to NIR upconverters upon excitation into the $^4I_{13/2}$ level, and they are the most widely applied Er^{3+}-doped host for the enhancement of silicon solar cells efficiency by UC.[5,6]

In this paper we present efficient IR to NIR and VIS UC emission for Er^{3+}-doped gadolinium oxysulfide, Gd_2O_2S: Er^{3+}. For the optimum Er^{3+}-concentration (10%) this material shows higher UC quantum yield than the most efficient Er^{3+}-doped β-$NaYF_4$ system upon monochromatic excitation into the $^4I_{13/2}$ level around 1500 nm. Luminescence, excitation, quantum yield, and lifetime measurements are reported for a series of Er^{3+}-doped Gd_2O_2S microcrystalline samples with different dopant concentrations, to achieve the highest UC efficiency and to provide insight in the mechanism responsible for the UC luminescence.

■ EXPERIMENTAL SECTION

Er^{3+}-doped Gd_2O_2S microcrystalline samples were custom-made for this research by Leuchtstoffwerk Breitungen GmbH (Breitungen, Germany), which has experience in the synthesis of high quality Gd_2O_2S doped with lanthanides for X-ray diagnostics. β-$NaYF_4$: Er^{3+} samples (hexagonal structure) were synthesized using the method described in ref 14 which is generally accepted to provide the most efficient UC materials. For comparison of the two hosts, the use of the highest quality β-$NaYF_4$: Er^{3+} UC system is required. The crystalline structure was confirmed by X-ray diffraction (XRD), the diffraction patterns were recorded using the Cu−Kα radiation (λ = 1.5418 Å) of a Philips 1700 diffractometer. The size and morphology of the samples were checked by using high resolution scanning electron microscopy (SEM) (Dual beam FEI Quanta 3D FEG SEM), by putting a thin layer of powder on conducting carbon tape.

Room temperature luminescence, excitation, and lifetime measurements in the VIS and IR range were performed using an optical parametric oscillator (OPO) system (Opotek HE 355 II) pumped by the third harmonic of a Nd:YAG laser as excitation source. This OPO system offers a continuous tunable optical range from 410 to 2400 nm,

dx.doi.org/10.1021/cm4005745 | Chem. Mater. 2013, 25, 1912−1921

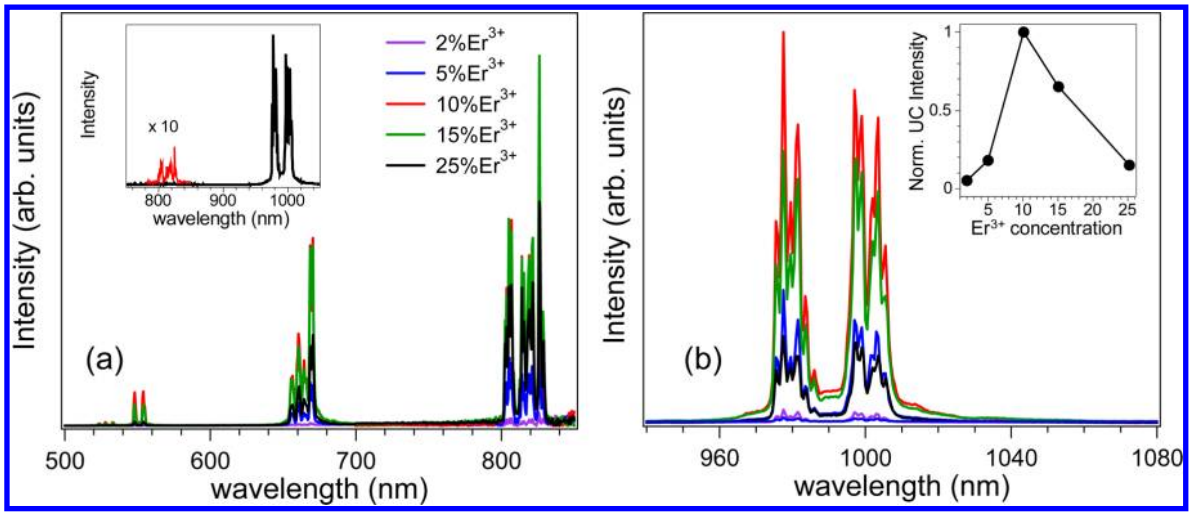

Figure 2. UC emission spectra of Gd_2O_2S doped with different Er^{3+} concentrations (2, 5, 10, 15, and 25%) upon pulsed excitation into the $^4I_{13/2}$ Er^{3+} level at 1510 nm. The inset in (a) compares the intensity of the NIR UC emissions at 990 and 820 nm. The inset in (b) shows the Er^{3+} concentration dependence of the integrated intensity of the UC emission bands.

with a maximum energy of 2 mJ per pulse in the IR, a pulse width of 10 ns, and a repetition rate of 20 Hz. Both the Hamamatsu R928 photomultiplier tube (PMT) and the N_2-cooled R5509-72 PMT detectors of the spectrofluorometer (Edinburgh Instruments FLS 920) were used for detection in the VIS and IR range, respectively, in luminescence and lifetime experiments. All emission spectra were corrected for the system response. Excitation spectra were recorded with a gated photon counter (Stanford Research Systems SR400), with typical gate width of 10 ms and a delay of 0.2 μs.

The external UC quantum yield was determined by dividing the number of emitted photons by the number of incident photons, while the internal UC quantum yield is given by the ratio of the number of emitted and absorbed photons. UC quantum yield experiments were carried out using two different and independent setups which gave within the experimental error the same results, and consequently reinforced the results found. First, at the Fraunhofer Institute for Solar Energy Systems an IR tunable laser (Santec ECL-210) was used as excitation source, and the UC emission light was collected via an optical fiber attached to the integrating sphere and guided to the spectrofluorometer (Princeton Instruments SP2300i) equipped with a CCD camera. Additionally, a silicon detector is applied on the integrating sphere to measure the integrated UC photon flux. The UC material was pressed against an optical window in a cylindrical powder cell and mounted on one side of an integrating sphere. The integrating sphere and detection setup were calibrated with a tungsten halogen lamp, with a precisely known emission spectrum. Thus, combining the two measurements the absolute emitted UC photon flux can be determined. The photon flux of the laser radiation was measured at the sample position with a calibrated germanium detector. The laser beam profile was determined with a InGaAs camera (Xenics, Xeva). The full area at half-maximum was used to calculate the irradiance of the excitation from the incident photon flux. Second, the UC quantum yield was measured at the Institute of Photonics and Quantum Sciences. Since the UC emission corresponding to the $^4I_{11/2} \rightarrow {}^4I_{15/2}$ transition around 1000 nm accounts for approximately 97% (depending on the excitation density) of the total UC emission, both external and internal UC quantum yield were measured for this transition, for different excitation power values up to 700 W/m^2. A supercontinuum laser (Fianium SC400 6W) was used with wavelength selection by a double monochromator for monochromatic excitation. A calibrated spectro fluorometer (Edinburgh Instruments FLS920) equipped with an integrating sphere (Jobin-Yvon) and a N_2-cooled NIR PMT (Hamamatsu R-5587) was used for detection. To measure the quantum yield a quartz cuvette filled with the microcrystalline powder was mounted at the focal point of the excitation light. The number of absorbed photons was determined by measuring the reduction in the intensity of the scattered IR excitation radiation for undoped β-$NaYF_4$ and Gd_2O_2S: 0.1%Er^{3+} in comparison to the highly Er^{3+}-doped samples. The number of emitted photons was determined from the integrated UC emission intensity. To determine the dependence of the UC quantum yield on pump power, both the UC quantum yield and the power density were recorded using various neutral-density filters in the excitation beam. The excitation beam power was measured using a calibrated germanium photodiode (Newport 818-IR), and the beam area was measured using an IR imaging camera (Electrophysics MicronViewer 7290A). A relative error of about 8% was estimated for the quantum yield values, primarily resulting from an error in the irradiance around 8% due to the uncertainty of the laser area and intensity profile.

RESULTS AND DISCUSSION

Structural Characterization. The XRD diffraction pattern of the β-$NaYF_4$: 25%Er^{3+} sample (not shown) is identical to those reported in ref 14 and confirms the presence of single phase β-$NaYF_4$. The β-$NaYF_4$ hexagonal structure is characterized by cation disorder, which gives rise to a variation in the coordination of the Er^{3+}-dopants. A XRD diffractogram obtained for Gd_2O_2S: 10%Er^{3+} is shown in Figure 1(a). The peak positions match perfectly with those of the trigonal phase of the oxysulfide (JCPDS card no. 00-026-1422). In Gd_2O_2S (trigonal structure, with $P\bar{3}m1$ space group) lanthanides replace Gd^{3+} ions at a 2d site (with C_{3v} point symmetry) surrounded by four oxygen and three sulfur ions, forming a seven coordinated geometry.[17] The maximum phonon energy in $NaYF_4$ is ~350 cm^{-1} and in Gd_2O_2S it is around 440 cm^{-1}.[18]

A comparison between the SEM images of Er^{3+}-doped Gd_2O_2S and $NaYF_4$ host materials is presented in Figure 1(b). SEM results demonstrate that the Gd_2O_2S sample has smaller particle size (2−10 μm) with well-separated particles, while the $NaYF_4$ sample shows bigger agglomerates of the crystallites up to over 100 μm in size. The smaller and more uniform crystallite size is advantageous for application of the Gd_2O_2S host material, since it facilitates the formation of a homogeneous UC layer, possibly in a polymer matrix, for combination with a solar cell. Besides, the Gd_2O_2S host has a high (thermal) stability and is not sensitive to moisture or oxygen, making it suitable for long-term application in solar cells.

dx.doi.org/10.1021/cm4005745 | Chem. Mater. 2013, 25, 1912−1921

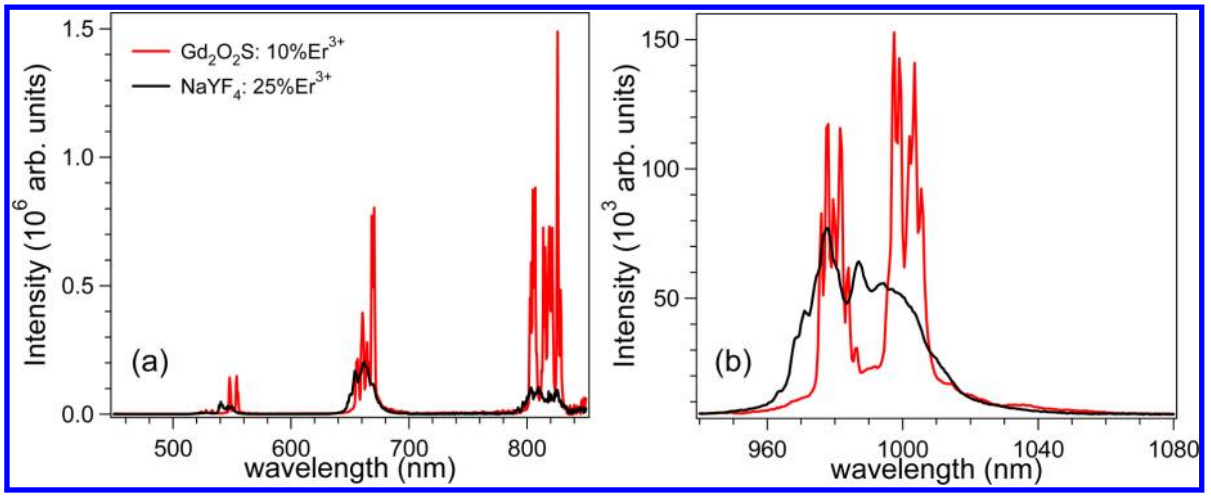

Figure 3. UC luminescence spectra of Gd_2O_2S: 10%Er^{3+} and β-$NaYF_4$:25%Er^{3+} after $^4I_{13/2}$ excitation at 1510 and 1523 nm, respectively. Note that the intensity scales are very different for (a) and (b), the NIR UC emission (b) is much stronger than the luminescence from higher excited states (a) (see also inset in Figure 2a).

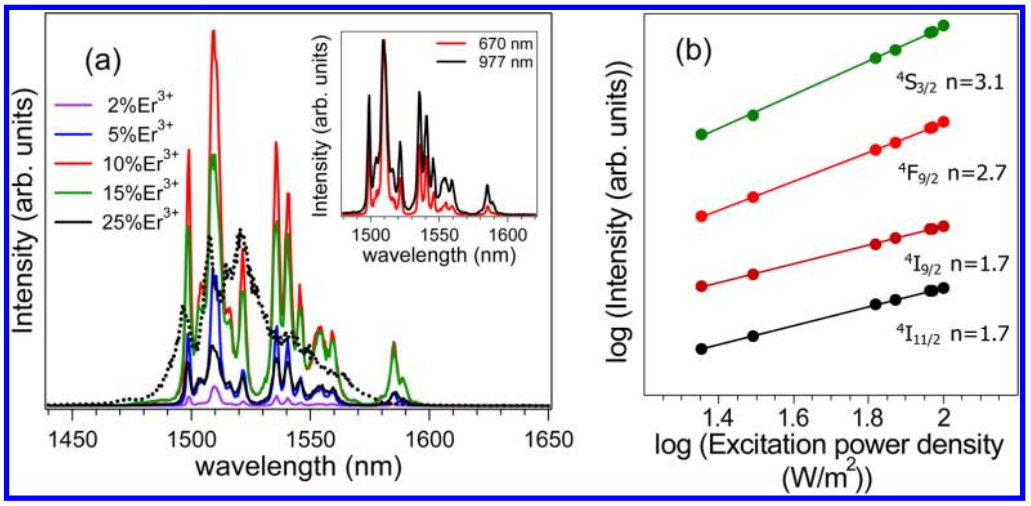

Figure 4. Excitation spectra of the NIR $^4I_{11/2} \rightarrow {}^4I_{15/2}$ Er^{3+} UC luminescence at 977 nm for Gd_2O_2S doped with 2, 5, 10, 15, and 25%Er^{3+} as well as β-$NaYF_4$: 25%Er^{3+} (dotted black line). The excitation spectra for the red $^4F_{9/2}$ and NIR $^4I_{11/2}$ Er^{3+} UC emission at 670.5 and 977 nm, respectively, are shown in the inset for Gd_2O_2S: 10%Er^{3+}. (b) Excitation power dependence of the intensity for all UC emission bands upon excitation at 1510 nm.

Upconversion Emission and Excitation Spectra. To evaluate the potential of the Er^{3+}-doped Gd_2O_2S system as UC material for the enhancement of silicon solar cell efficiency, we compare the UC emission and excitation spectra for Er^{3+}-doped Gd_2O_2S with different Er^{3+} concentrations to determine the optimum concentration. This material is then compared with β-$NaYF_4$ doped with 25% Er^{3+}, the optimum doping concentration for $NaYF_4$.

The UC emission spectra of Er^{3+}-doped Gd_2O_2S were measured for different Er^{3+} concentrations upon pulsed excitation into the maximum of the $^4I_{13/2}$ excitation band at 1510 nm (Figure 2). The emission bands observed around 540, 660, and 820 nm are assigned to transitions from the $^4S_{3/2}$, $^4F_{9/2}$, and $^4I_{9/2}$ excited states to the $^4I_{15/2}$ ground state of the Er^{3+}. The emission peaks around 990 nm correspond to the $^4I_{11/2} \rightarrow {}^4I_{15/2}$ Er^{3+} transition. The intensity scale is different for the VIS and IR range. Scaling of the emission spectra reveals that the NIR $^4I_{11/2}$ UC luminescence around 990 nm dominates, and represents around 97% of the overall UC emission intensity (see inset in Figure 2a). At higher excitation densities the relative contribution of the VIS emission is higher, but the 990 nm emission is always dominant. The luminescence spectra in Figure 2 show that the UC intensity strongly increases upon increasing the Er^{3+} concentration from 2 to 10%. The increase is supralinear, and the highest UC luminescence is observed for the sample doped with 10% Er^{3+} (see inset in Figure 2b). The decrease of the UC emission intensity for higher Er^{3+} concentrations can be ascribed to concentration quenching due to cross-relaxation processes and energy migration over the Er^{3+}-sublattice to defects.[19] Concentration quenching is commonly observed for luminescent systems and depends strongly on the quality of the materials achieved with the synthesis process.[20] Optimizing the synthesis procedure leads to fewer defects and higher luminescence intensities. It is also dependent on the nature of the host lattice. Some hosts are easier to prepare with a low concentration of defects than others. The influence of synthesis procedures and the role of lattice defects on the luminescence efficiency are still poorly understood and yet it is very

dx.doi.org/10.1021/cm4005745 | Chem. Mater. 2013, 25, 1912−1921

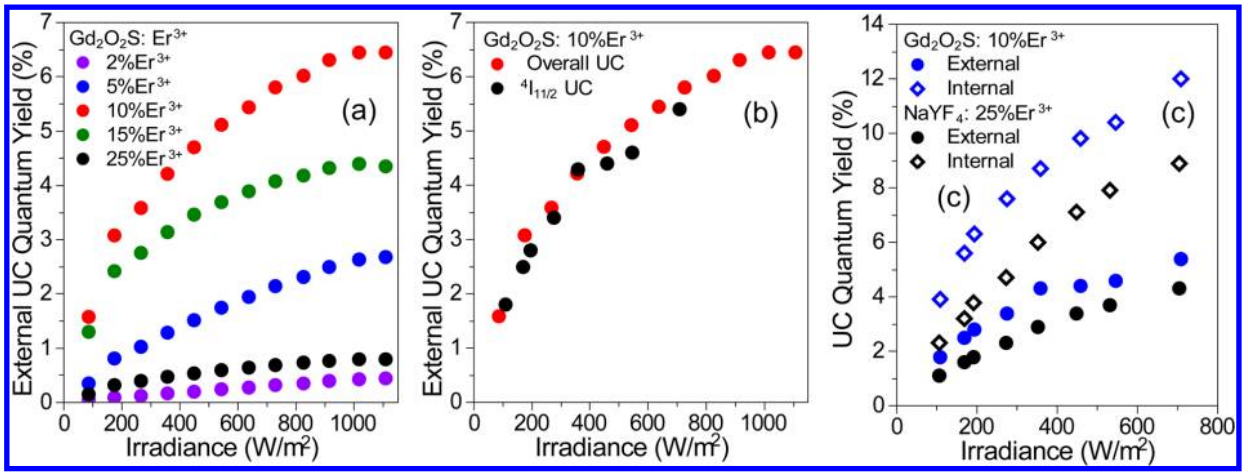

Figure 5. (a) External UC quantum yield of Er^{3+}-doped Gd_2O_2S for 2, 5, 10, 15, and 25% doping concentrations measured at different irradiances for an excitation wavelength of 1510 nm. (b) Comparison between the total and $^4I_{11/2}$ external UC quantum yields in Gd_2O_2S: 10%Er^{3+} for different excitation powers at 1510 nm, measured with different setups (red dots from Fraunhofer Institute for Solar Energy Systems and black dots from Institute of Photonic and Quantum Sciences). (c) Power dependence of the external and internal $^4I_{11/2}$ UC quantum yield in Gd_2O_2S: 10%Er^{3+} and β-$NaYF_4$: 25%Er^{3+}, upon excitation at 1510 and 1523 nm, respectively.

important for the application and optimization of luminescent materials.[21]

The UC luminescence properties of the most efficient Gd_2O_2S: 10%Er^{3+} sample are compared to those of the well-known β-$NaYF_4$: 25%Er^{3+} UC system for excitation into the $^4I_{13/2}$ state. The emission spectra recorded under identical conditions, for pulsed excitation at the wavelength of maximum absorption, 1510 nm for Gd_2O_2S: 10%Er^{3+} and 1523 nm for β-$NaYF_4$: 25%Er^{3+}, are shown in Figure 3. The total intensity of the UC emission bands is higher for Gd_2O_2S: 10%Er^{3+} in comparison with β-$NaYF_4$: 25%Er^{3+} samples, and the intensity ratio between the emission peaks from different excited states also depends on the host. An increase in the NIR UC emission intensity by a factor of 2 is measured for Gd_2O_2S: 10%Er^{3+} compared to β-$NaYF_4$: 25%Er^{3+}. The UC luminescence enhancement is even stronger for emission bands at shorter wavelengths (higher energies), where the intensity of the Er^{3+} UC emission in Gd_2O_2S is 1 order of magnitude higher than in β-$NaYF_4$. Pulsed excitation makes it difficult to accurately measure UC quantum yields. Therefore, in the next section the UC quantum yields under continuous wave excitation will be determined as a function of the excitation power for both systems, confirming the present observation. Note that the emission spectra for Er^{3+}-doped Gd_2O_2S show sharp well-defined emission lines due to transitions between specific crystal field components of both the excited state and the ground state. On the contrary, for β-$NaYF_4$: Er^{3+} the emission is broadened. This has been observed before and is explained by the cation disorder in the crystal structure which renders less well-defined crystallographic sites.[16] The variation in local surroundings gives rise to slightly different crystal field splittings and broadening of the spectral lines similar to but not as pronounced as in glasses.

Figure 4a shows the excitation spectra of the NIR $^4I_{11/2} \rightarrow {}^4I_{15/2}$ Er^{3+} UC luminescence at 977 nm in the $^4I_{15/2} \rightarrow {}^4I_{13/2}$ Er^{3+} region around 1500 nm for different Gd_2O_2S samples doped with 2, 5, 10, 15, and 25% Er^{3+}. The UC excitation spectrum of β-$NaYF_4$: 25%Er^{3+} for 978 nm UC emission is also shown for comparison (dotted line). The observed trend is analogous to the behavior observed for the UC emission intensity. The Gd_2O_2S: 10%Er^{3+} is the most efficient system among the samples studied under the present excitation conditions. The UC excitation spectrum in β-$NaYF_4$: 25% Er^{3+} shows pronounced line broadening in comparison to the sharp line spectra measured for the Gd_2O_2S: Er^{3+} samples, similar to the UC emission spectra (Figure (3)). The relative intensity of the excitation lines for the most efficient Gd_2O_2S: 10%Er^{3+} sample is about two times higher than for the β-$NaYF_4$: 25%Er^{3+} system, again in agreement with the results for the UC emission spectra. The inset in Figure 4a compares the excitation spectra for the NIR $^4I_{11/2}$ UC emission at 977 nm and the red $^4F_{9/2}$ UC emission at 670.5 nm. As expected, the peak positions are the same and correspond to transitions from different crystal field components of the $^4I_{15/2}$ ground state to crystal field components in the $^4I_{13/2}$ excited state. There is a difference in the shape of the excitation bands for the red and NIR UC emissions. The lines in the excitation spectrum of the $^4F_{9/2} \rightarrow {}^4I_{15/2}$ emission are narrower than the ones of the $^4I_{11/2} \rightarrow {}^4I_{15/2}$ UC luminescence. The reduction of the bandwidth is related to the number of photons involved in the energy transfer UC (ETU) mechanisms responsible for the emission bands originating from different excited states. For a higher order process, sharper lines are expected since the intensity depends on the number of photons absorbed to a higher power.[22] The number of photons required to populate the different excited states can be estimated from the slope in the pump power dependence of the UC emission intensity.[23]

Figure 4b shows the UC luminescence intensity versus the excitation power density on a double logarithmic scale for the $^4S_{3/2} \rightarrow {}^4I_{15/2}$ (540 nm), $^4F_{9/2} \rightarrow {}^4I_{15/2}$ (660 nm), $^4I_{9/2} \rightarrow {}^4I_{15/2}$ (820 nm), and $^4I_{11/2} \rightarrow {}^4I_{15/2}$ (990 nm) Er^{3+} emission in Gd_2O_2S: 10%Er^{3+} after excitation at 1510 nm. The measured slopes for the emission bands at 540, 660, 820, and 990 nm are 3.1, 2.7, 1.7, and 1.7, respectively. This observation suggests that the UC luminescence from $^4I_{11/2}$ and $^4I_{9/2}$ excited states involves a two photon process, while at least three photons are involved in the red $^4F_{9/2} \rightarrow {}^4I_{15/2}$ and green $^4S_{3/2} \rightarrow {}^4I_{15/2}$ UC emissions. The dependence on the second and third power of the excitation power, for the $^4I_{11/2}$ and $^4F_{9/2}$ UC emissions, explains the narrowing of the excitation spectrum of the emission at 670.5 nm compared to the spectrum detecting at 977 nm (inset in Figure 4a).

dx.doi.org/10.1021/cm4005745 | Chem. Mater. 2013, 25, 1912−1921

Upconversion Quantum Yield. For application of UC materials the quantum yield of the UC process is an important parameter. Measuring the UC quantum yield is not easy, and comparison of UC quantum yields reported requires the knowledge of the irradiance of the excitation. For low irradiance values the UC quantum yield (for a two-photon UC process) is proportional to the irradiance, while it saturates at higher incident irradiance values. To determine and compare the quantum yield for IR to NIR UC in Er^{3+}-doped β-$NaYF_4$ and Gd_2O_2S, the dependence of the UC quantum yield of the various materials on the irradiance was measured under continuous-wave excitation. In Figure 5a the irradiance dependence of the external UC quantum yield for Gd_2O_2S samples doped with different Er^{3+} concentration upon monochromatic excitation at 1510 nm is displayed. Contributions of all the UC emission bands from the $^4S_{3/2}-^2H_{11/2}$, $^4F_{9/2}$, $^4I_{9/2}$, and $^4I_{11/2}$ excited states to the ground state are included. These results are in good agreement with the UC luminescence and excitation experiments (Figures 2 and 4), and confirm that 10% Er^{3+} doping is the optimum concentration for efficient UC. The total external quantum yield for the NIR and VIS UC emissions is 6.5 ± 0.5% under 1510 nm excitation with 1100 W/m^2. Figure 5b compares the external UC quantum yield in Gd_2O_2S: 10%Er^{3+} considering UC emissions from all Er^{3+} excited states, and the UC emission from the $^4I_{11/2}$ level only, measured with different experimental setups. The overall UC quantum yield was measured with the setup at the Fraunhofer Institute for Solar Energy Systems while the $^4I_{11/2}$ UC quantum yield was measured at the Institute of Photonic and Quantum Sciences. The quantum yield for the NIR $^4I_{11/2}$ UC emission centered at 990 nm is similar to the total UC quantum yield at low excitation densities. The $^4I_{11/2}$ UC emission represents around 94% of the total UC luminescence for excitation powers below 450 W/m^2. At higher excitation densities the contribution from the VIS UC emission increases, consistent with the expected increase of the relative contribution of higher order (three photon) processes at higher excitation densities. This observation corroborates the finding reported in the previous section where the $^4I_{11/2}$ UC emission contributes around the 97% to the total UC luminescence under pulsed excitation. Moreover, the results presented in Figure 5b also give evidence for the good agreement of the quantum yield values obtained with two completely different setups.

To compare the UC luminescence of Er^{3+}-doped Gd_2O_2S and β-$NaYF_4$, the internal and external UC quantum yields of the $^4I_{11/2}$ UC emission were determined for both hosts doped with the optimum Er^{3+} concentration (10% for Gd_2O_2S and 25% for β-$NaYF_4$). Figure 5c shows both the external and the internal $^4I_{11/2}$ UC quantum yields for Gd_2O_2S: 10%Er^{3+} and β-$NaYF_4$: 25%Er^{3+} under excitation at 1510 and 1523 nm, respectively. The wavelengths of 1510 and 1523 nm correspond to the maxima in the UC excitation spectra for the two hosts. The maximum internal UC quantum yield is 12.0 ± 1.0% for Gd_2O_2S: 10%Er^{3+}, and 8.9 ± 0.7% for β-$NaYF_4$: 25%Er^{3+}, under monochromatic excitation at 700 W/m^2, showing that the UC quantum yield is higher for Er^{3+}-doped Gd_2O_2S. The quantum yield is still increasing with laser power, indicating that higher absolute quantum yields can be achieved.

There are only a few studies on the quantum yield of Er^{3+} UC luminescence upon excitation into the $^4I_{13/2}$ level.[5,6,12,24] In fact, the excitation power dependence of the UC quantum yield in Er^{3+}-doped Gd_2O_2S is presented in this work for the first time. The external UC quantum yield value measured here for β-$NaYF_4$: 25%Er^{3+} (4.3% at 700 W/m^2) is in line with the UC quantum yield previously published for this material under monochromatic excitation (5.1% at 1880 W/m^2), which was the highest value reported so far.[6] The higher literature value was achieved for a higher excitation density, confirming that at 700 W/m^2 the UC quantum yield still increases with laser power. The values obtained here are an order of magnitude higher than those published for $LiYF_4$: 10%Er^{3+} nanoparticles by Chen et al., about 1.2 ± 0.1% for much higher excitation power (1.5 × 10^6 W/m^2).[12] A higher quantum yield of 16.2 ± 0.5% was achieved for Er^{3+}-doped β-$NaYF_4$ under high power broadband excitation (80 nm) at (2.3 ± 0.1) × 10^6 W/m^2.[24] On the basis of this comparison, it is clear that the UC quantum yield reported here for Gd_2O_2S: 10%Er^{3+} under monochromatic excitation is the highest ever measured for IR to NIR UC. Evaluation of the UC quantum yield in high quality Gd_2O_2S: Er^{3+} and β-$NaYF_4$: Er^{3+} shows that the oxysulphide host is superior for achieving high UC quantum yields under monochromatic excitation.

Discussion of the Upconversion Quantum Yield. It is interesting to try and understand the high UC quantum yield in Gd_2O_2S: Er^{3+} and β-$NaYF_4$: Er^{3+}. There are a number of factors that are considered to yield intense UC luminescence. Low phonon frequency, high absorption strengths, spectral width, equidistant energy levels, resonance for energy transfer steps, and long-lived intermediate states are all factors that contribute. In addition, the presence of defects leading to luminescence quenching is an important factor, which however is difficult to quantify. We will discuss the various factors for the two materials, β-$NaYF_4$: Er^{3+} and Gd_2O_2S: Er^{3+}.

The maximum phonon energy in Gd_2O_2S and $NaYF_4$ lattices is around 440 and 350 cm^{-1}, respectively. The higher phonon frequency indicates that nonradiative multiphonon relaxation processes have a higher probability in the oxysulfide than in the fluoride host material. This may lead to the assumption that the UC quantum yield will be lower in the oxysulphide. However, to determine if higher phonon energy leads to stronger quenching of the emission by multiphonon relaxation it is important to also consider the energy gaps to the next lower level for the emitting states. In case more than six phonons are needed to bridge the gap, multiphonon relaxation has a very low probability and radiative decay will dominate. For different emitting Er^{3+} excited states the gap is at least six times the maximum phonon energy in both Gd_2O_2S and $NaYF_4$, except for the $^4I_{9/2}-^4I_{11/2}$ gap. The most important gap here is the one for the $^4I_{11/2}$ level, from which over 97% of the UC emission originates. The gap to the $^4I_{13/2}$ next lower level is 3500 cm^{-1} which corresponds to 8 phonons in Gd_2O_2S and 10 phonons in $NaYF_4$, making losses due to multiphonon relaxation negligible in both materials. Only in hosts with phonon energies above ~600 cm^{-1} will multiphonon relaxation start to contribute to lowering the UC emission. Note that phonons also play an important role in making the UC process efficient as phonon assistance is required in the ETU process. The energy of the lowest $^4I_{13/2}$ crystal field component (~6400 cm^{-1}) is slightly more than half the energy of the $^4I_{9/2}$ excited state (~12 500 cm^{-1}). The energy mismatch (~300 cm^{-1}) can be easily made up by phonon emission making the ETU process a one-phonon assisted energy transfer process.

The excitation spectral bandwidth determines the range over which IR radiation can be absorbed. There are two factors that are relevant. The crystal field splitting will determine the total width of the region in which radiation can be absorbed.

dx.doi.org/10.1021/cm4005745 | Chem. Mater. 2013, 25, 1912−1921

Inhomogeneous broadening contributes to a better absorption between the absorption peaks. According to the stronger crystal field in oxides comparing to halides, a broader absorption range is expected in Gd_2O_2S than in $NaYF_4$ because of the larger crystal field splitting of the energy levels. However, the broadening of the UC emission and excitation spectra observed for Er^{3+}-doped β-$NaYF_4$ is due to the presence of disorder around different sites for Er^{3+} ions in this host lattice.[16] For the present study, the width of the excitation peaks is not relevant, since UC emission is measured upon monochromatic excitation. However, for application in solar cells the large inhomogeneous broadening as observed for β-$NaYF_4$: Er^{3+} is favorable, since a larger fraction of the broad solar spectrum would be resonant with the $^4I_{15/2} \rightarrow {}^4I_{13/2}$ transitions in Er^{3+} ions.[24]

The role of the absorption strength for transitions between the various levels is to enhance the absorption from the ground state, and also to increase energy transfer rates between neighboring ions. The absorption strength of lanthanide ions increases in more covalent lattices because of stronger admixture of opposite parity. Higher absorption strengths are thus expected for Er^{3+} in Gd_2O_2S than in $NaYF_4$. This is consistent with the much lower optimum Er^{3+} concentration for UC in Gd_2O_2S (10%) in comparison to $NaYF_4$ (25%). A much higher Er^{3+}-concentration is required in $NaYF_4$ to achieve a sufficiently strong IR absorption. At the same, the more efficient energy transfer between Er^{3+} neighbors in Gd_2O_2S will lead to concentration quenching at lower Er^{3+}-concentrations. To quantify the difference in oscillator strengths, the emission lifetimes of the different Er^{3+} excited states in Gd_2O_2S and β-$NaYF_4$ UC materials were obtained by recording the luminescence decay times of the emitting levels for samples doped with very low Er^{3+} concentration, Gd_2O_2S: 0.1%Er^{3+} and β-$NaYF_4$: 0.1%Er^{3+}. The best fittings to a single exponential decay curve are shown in Table 1. The lifetime for emission

Table 1. Lifetimes of Er^{3+} Excited States in Gd_2O_2S: 0.1% Er^{3+} and β-$NaYF_4$: 0.1%Er^{3+} Measured after Direct Excitation in the Emitting Level

emitting state	$\tau(Gd_2O_2S$: 0.1%$Er^{3+})$	$\tau(\beta$-$NaYF_4$: 0.1%$Er^{3+})$
$^4S_{3/2}$–$^2H_{11/2}$	560 ± 20 μs	3.25 ± 0.05 ms
$^4F_{9/2}$	100 ± 1 μs	675 ± 5 μs
$^4I_{9/2}$	17.5 ± 0.5 μs	23 ± 1 μs
$^4I_{11/2}$	2.30 ± 0.05 ms	11.2 ± 0.1 ms
$^4I_{13/2}$	3.7 ± 0.1 ms	11.8 ± 0.1 ms

from the $^4I_{9/2}$ level is short due to fast nonradiative multiphonon relaxation. The lifetimes for the other emissions are dominated by radiative decay and are 4 to 7 times shorter for Er^{3+} in Gd_2O_2S. This is consistent with higher oscillator strengths for Er^{3+} in Gd_2O_2S compared to Er^{3+} in β-$NaYF_4$. The higher oscillator strengths lead to increased absorption strengths as well as higher energy transfer rates which gives rise to more efficient upconversion at lower Er^{3+} concentrations.

A final and probably the most important factor that contributes to the high UC quantum yield is the absence of quenching by defects and impurities. It is well-known in the synthesis of efficient phosphors that the synthesis procedure is crucial for obtaining highly luminescent materials. For example, by optimizing synthesis procedures for commercial down-shifting lamp phosphors quantum yields over 90% have been realized. The same material synthesized by a standard procedure often has quantum yields below 30%. Competing absorption by impurities in the ultraviolet and energy transfer from the emitting state to defects are known to contribute to lower the quantum efficiency in lamp phosphors.[25] Optimizing synthesis procedures, which involves a certain amount of trial and error, leads to realization of high quantum yields; however, the exact nature and the role of defects and impurities is not well understood. For the present hosts, β-$NaYF_4$ and Gd_2O_2S, optimized synthesis procedures have been used. For example, elimination of OH^-, which is a well-known quencher of IR emission by multiphonon relaxation, is important to realize high UC quantum yield in β-$NaYF_4$: Er^{3+}.[26] Efficient IR to NIR UC can in principle be expected in many hosts with maximum phonon energies below 600 cm^{-1} if the materials can be synthesized with a low concentration of defects and impurities. The present lack of understanding on the role, the nature, and the formation of defects and impurities that contribute to quenching of IR and NIR emission, makes it impossible to predict or explain which of many low-phonon hosts will give the highest UC quantum yields.

Upconversion Mechanisms under $^4I_{13/2}$ Excitation. The mechanisms responsible for the efficient VIS and NIR UC luminescence in Er^{3+}-doped Gd_2O_2S or β-$NaYF_4$ after $^4I_{13/2}$ excitation have not been previously described in detail in the literature. An insightful method to unravel UC mechanisms is studying the time dependence of the UC emission intensity upon pulsed excitation.

The temporal evolution of the Er^{3+} UC luminescence intensity from different excited states, $^4I_{11/2}$, $^4I_{9/2}$, $^4F_{9/2}$, and $^4S_{3/2}$-$^2H_{11/2}$ in Gd_2O_2S: 10%Er^{3+} upon ns pulsed excitation at 1510 nm into the $^4I_{13/2}$ level is shown in Figure 6. The lengthening of the UC emission lifetime compared to the lifetime after direct excitation (see Table 1) indicates that the UC luminescence decay is affected by the long lifetime of the metastable $^4I_{13/2}$ Er^{3+} level that feeds the UC emission. Moreover, the differences in the time dependence for different UC emissions are relevant to identify the mechanisms responsible for the UC luminescence.

An immediate decay of the emission intensity after the excitation pulse (without a rise) points toward ground state absorption followed by excited state absorption (GSA/ESA) where during the excitation pulse the high excited state is reached by absorption of two photons. If the temporal dependence of the UC emission shows an initial rise followed by a decay, the dominant mechanism is energy transfer UC (ETU). The rise time is influenced by both the energy transfer processes and the lifetime of the emitting state. The decay reflects the slow feeding of the high excited state by energy transfer between two excited Er^{3+} ions, which brings one ion to a higher excited state (giving rise to UC emission) and the other ion to a lower excited state (usually the ground state). The temporal evolution of the UC emission intensity as a function of time after the short IR excitation pulse can be fitted to a Vial's type equation:[27]

$$I(t) = Ae^{-t/\tau_D} - Be^{-t/\tau_R} \quad (1)$$

where τ_D and τ_R represent the decay and rise of the transient, respectively. τ_D is essentially the UC luminescence lifetime, which is influenced by the lifetime of the emitting level and the lifetime of the levels feeding the excited state through the energy transfer process. The rise time τ_R is determined by the lifetime of the emitting state and the ETU transfer rate, W_{ETU}.

dx.doi.org/10.1021/cm4005745 | Chem. Mater. 2013, 25, 1912–1921

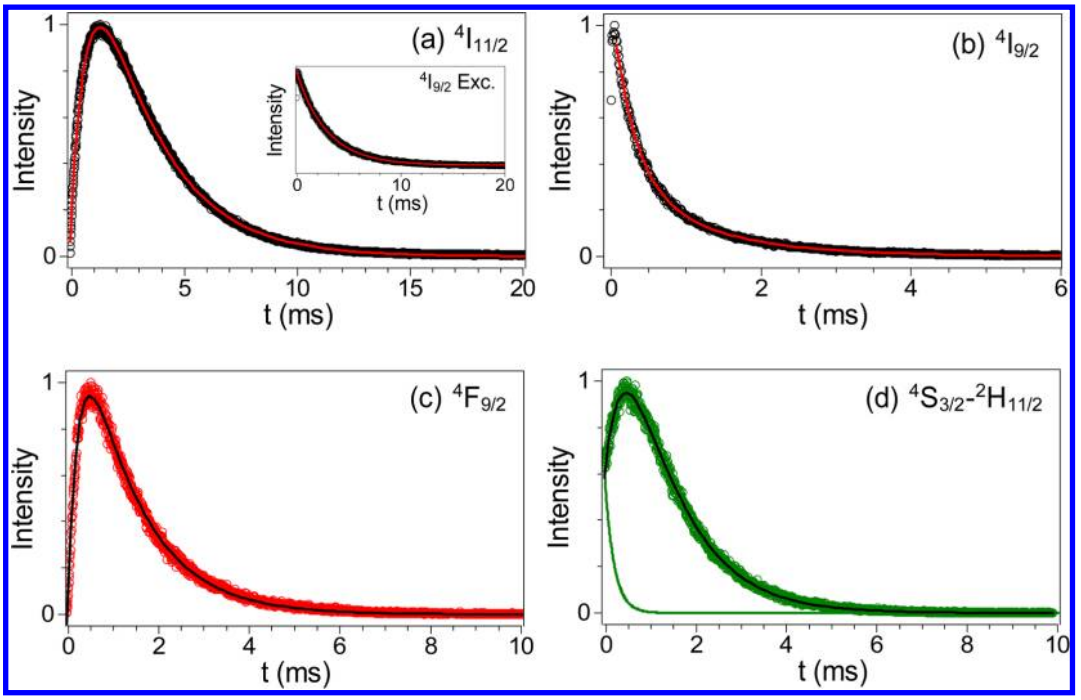

Figure 6. Luminescence decay curves of the Er^{3+} UC emission intensity from the $^4I_{11/2}$ (a), $^4I_{9/2}$ (b), $^4F_{9/2}$ (c), and $^4S_{3/2}-^2H_{11/2}$ (d) excited states in Gd_2O_2S: 10%Er^{3+} after pulsed excitation into the $^4I_{13/2}$ level at 1510 nm. The inset in (a) shows the temporal dependence of the $^4I_{11/2}$ emission upon excitation into the $^4I_{9/2}$ level at 825 nm. The green line in (d) corresponds to the GSA/ESA contribution to the $^4S_{3/2}-^2H_{11/2}$ UC emission (see text). Drawn red or black lines are the results of different fitting procedures (Vial's procedure (eq 1) or exponential decay, see text).

Table 2. Decay and Rise Lifetimes of the $^4S_{3/2}-^2H_{11/2}$, $^4F_{9/2}$, and $^4I_{11/2}$ Er^{3+} UC Emissions in Gd_2O_2S: 10%Er^{3+} after Pulsed Excitation at 1510 nm. The Values for the Rise and Decay have been Determined Using a Vial's Type Fitting (eq 1). The $^4I_{9/2}$ Emission Decay Curve was Fitted to a Bi-exponential Decay

emitting state	τ_D	τ_R
$^4S_{3/2}-^2H_{11/2}$	1.08 ± 0.02 ms	460 ± 10 μs
$^4F_{9/2}$	1.20 ± 0.02 ms	240 ± 10 μs
$^4I_{9/2}$	$\tau1$ = 285 ± 10 μs	
	$\tau2$ = 1.12 ± 0.05 ms	
$^4I_{11/2}$	2.68 ± 0.02 ms	770 ± 10 μs

Table 3. Decay and Rise Lifetimes of Different Er^{3+} UC Emissions in β-$NaYF_4$: 25%Er^{3+} after Excitation at 1523 nm Using Either Single Exponential Decay or a Vial's Type Model (eq 1)

emitting state	τ_D	τ_R
$^4S_{3/2}-^2H_{11/2}$	$\tau1$ = 0.53 ± 0.02 ms	
	$\tau2$ = 5.7 ± 0.1 ms	
$^4F_{9/2}$	3.77 ± 0.02 ms	2.55 ± 0.02 ms
$^4I_{9/2}$	3.85 ± 0.03 ms	
$^4I_{11/2}$	9.10 ± 0.05 ms	3.29 ± 0.03 ms

The luminescence decay curve for the main UC emission $^4I_{11/2} \rightarrow {}^4I_{15/2}$ for pulsed excitation at 1510 nm is shown in Figure 6a. The $^4I_{11/2}$ UC emission shows an initial rise of 770 μs followed by a 2.7 ms decay (Table 2). The rising part starts from zero intensity which indicates that ETU dominates. To verify that the rise is not due to slow feeding by multiphonon relaxation from the $^4I_{9/2}$ level which can be reached by absorption of two 1510 nm photons, the luminescence decay curve of the $^4I_{11/2}$ emission was also recorded after direct excitation into the $^4I_{9/2}$ level (shown in the inset in Figure 6a). No rise time is observed, confirming that the observed rise time upon pulsed IR excitation is due to ETU. A decay time of 2.80 ± 0.05 ms was measured; this value is similar to the decay time of the $^4I_{11/2}$ UC emission after excitation at 1510 nm (see Table 2). The UC emission from the $^4I_{9/2}$ level after 1510 nm excitation (Figure 6b) shows an almost immediate decay with a two exponential decay behavior (τ_1 = 285 ± 10 μs, τ_2 = 1.12 ± 0.05 ms (see Table 3)). The absence of a slow rise time suggests that GSA/ESA is the UC mechanism. This would be very surprising since the $^4I_{11/2}$ emission is fed via the $^4I_{9/2}$ level. ETU between two neighboring Er^{3+} ions already in the $^4I_{13/2}$ excited state leads to population of the $^4I_{9/2}$ level, which then relaxes fast by multiphonon relaxation to the $^4I_{11/2}$ level, yielding the strong UC emission at 1000 nm. Moreover, the decay time observed for the $^4I_{9/2}$ UC luminescence after excitation at 1510 nm is much longer than the intrinsic lifetime (see Tables 1 and 3). After GSA/ESA population, the emitting state should decay with the intrinsic lifetime; therefore, the lengthening of the decay time points out the contribution of the ETU mechanism to the population of the $^4I_{9/2}$ state. The fast rise time observed for the $^4I_{9/2}$ UC emission is due to the fast multiphonon relaxation from this level to the lower lying $^4I_{11/2}$ level, which explains also the fast decay of the $^4I_{9/2}$ state observed under direct excitation (see Table 1).

For the $^4F_{9/2} \rightarrow {}^4I_{15/2}$ transition (Figure 6c) a rising part precedes the decay and the rise is starting from zero, again indicating a dominant ETU mechanism. The values for rise and decay times after fitting to a Vial's type equation are shown in Table 2. In contrast, the rise of the $^4S_{3/2}-^2H_{11/2}$ UC luminescence intensity is not starting from zero (Figure 6d), which implies that besides the ETU process, there is also a contribution of a GSA/ESA mechanism within a single Er^{3+} ion.

dx.doi.org/10.1021/cm4005745 | Chem. Mater. 2013, 25, 1912−1921

Considering that the lifetime of the $^4S_{3/2}$–$^2H_{11/2}$ emission in the GSA/ESA process should be the same as the one measured after direct excitation, it is possible to estimate the GSA/ESA and GSA/ETU contribution to the total intensity.[28] The area under the exponential decay with the intrinsic $^4S_{3/2}$–$^2H_{11/2}$ lifetime in Gd_2O_2S: 10%Er^{3+} (560 μs) (green line in Figure 6d) represents the GSA/ESA component. Hence, contributions of 93% and 7% were determined for GSA/ETU and GSA/ESA mechanisms, respectively. The decay and rise lifetimes for the green $^4S_{3/2}$ Er^{3+} UC emission are also shown in Table 2.

The Er^{3+} energy levels as well as the mechanisms explaining the Er^{3+} UC luminescence in Gd_2O_2S: 10%Er^{3+} are shown in Figure 7. After excitation at 1510 nm, Er^{3+} ions are promoted to the $^4I_{13/2}$ first excited state. Population of higher Er^{3+} excited states can be realized by different processes. An Er^{3+} ion can be promoted to the $^4I_{9/2}$ excited state, from where emission around 820 nm occurs, via the $^4I_{13/2} \rightarrow {}^4I_{9/2}$ ESA and mainly the ($^4I_{13/2}$, $^4I_{13/2}$) → ($^4I_{15/2}$, $^4I_{9/2}$) ETU processes. Considering the short lifetime of the $^4I_{9/2}$ Er^{3+} state (around 16 μs, see Table 1) and the small energy gap between $^4I_{9/2}$ and $^4I_{11/2}$ levels (around 2000 cm^{-1}) it is clear that fast multiphonon relaxation to the $^4I_{11/2}$ level occurs. The ($^4I_{13/2}$, $^4I_{13/2}$) → ($^4I_{15/2}$, $^4I_{9/2}$) ETU process followed by the $^4I_{9/2} \rightarrow {}^4I_{11/2}$ multiphonon relaxation is responsible for the main $^4I_{11/2}$ UC emission in Gd_2O_2S: Er^{3+}. Note that the ($^4I_{13/2}$, $^4I_{13/2}$) → ($^4I_{15/2}$, $^4I_{11/2}$) ETU mechanism is not possible in view of the large energy mismatch (~3000 cm^{-1}).

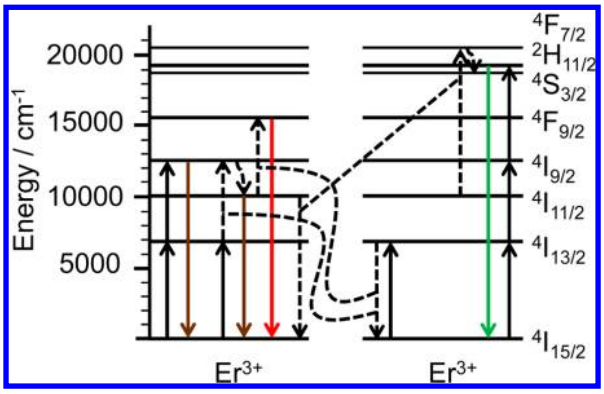

Figure 7. Er^{3+} energy level scheme with the observed luminescence transitions and the proposed UC mechanisms. Drawn black lines indicate absorption of 1510 nm IR photons. Straight broken lines indicate energy transfer processes between neighboring Er^{3+} ions and colored lines indicate emission of NIR (brown), red and green emission. The short curved broken lines denote fast multiphonon relaxation.

Additionally, after the population of the $^4I_{11/2}$ Er^{3+} level, the $^4F_{9/2}$ Er^{3+} emitting state is populated via the ($^4I_{11/2}$, $^4I_{13/2}$) → ($^4F_{9/2}$, $^4I_{15/2}$) ETU process giving rise to red UC emission bands centered at 660 nm. Because of the large energy mismatch (~1500 cm^{-1}) this process is not very efficient. Population of the $^4F_{9/2}$ level is only possible through ETU and not by multiple resonant absorption steps during the excitation pulse, consistent with the experimentally measured decay curve with a rise starting from zero intensity. For the $^4S_{3/2}$–$^2H_{11/2}$ UC emission, the experimentally measured decay curve does suggest a contribution from direct excitation during the excitation pulse. Indeed the $^2H_{11/2}$ state is reached by a second ESA process within the laser pulse, upon absorption of a 1510 nm photon by an Er^{3+} ion in the $^4I_{9/2}$ state. But the ($^4I_{11/2}$, $^4I_{11/2}$) → ($^4F_{7/2}$, $^4I_{15/2}$) ETU mechanism followed by nonradiative decay leads to the main population of the $^4S_{3/2}$–$^2H_{11/2}$ state. Then, the radiative decay to the ground state generates green UC luminescence around 540 nm. ETU processes leading to population of the $^4F_{9/2}$ and $^4S_{3/2}$–$^2H_{11/2}$ excited states involve three and four photons, respectively, in

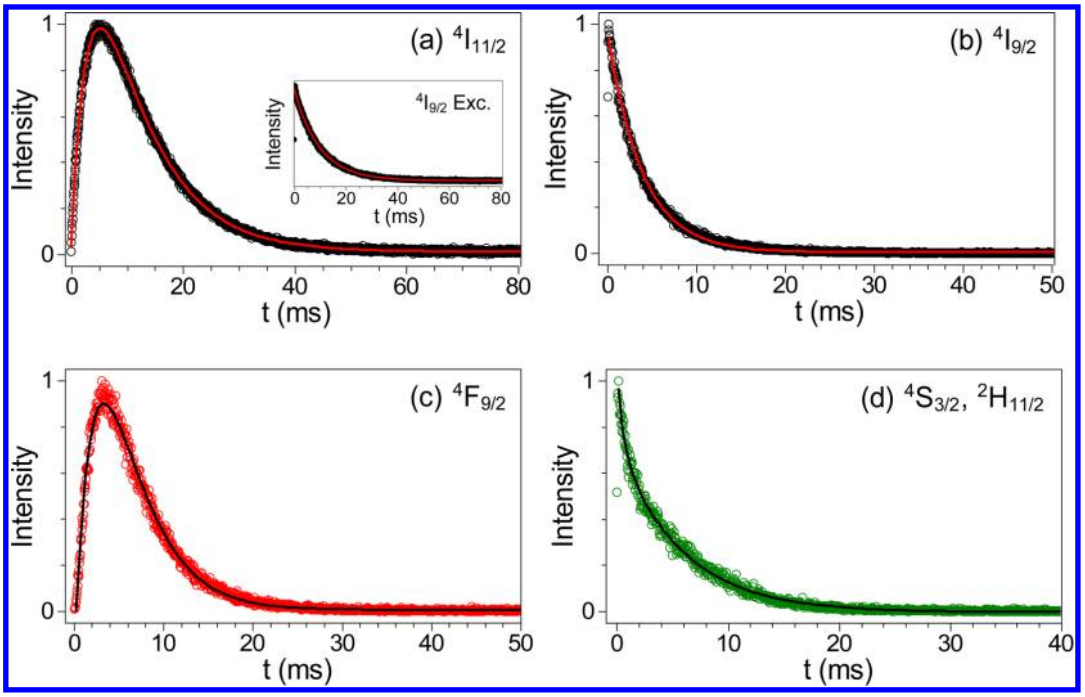

Figure 8. Temporal evolution of the Er^{3+} UC luminescence intensity from the $^4I_{11/2}$ (a), $^4I_{9/2}$ (b), $^4F_{9/2}$ (c), and $^4S_{3/2}$–$^2H_{11/2}$ (d) excited states, in β-$NaYF_4$: 25%Er^{3+} after pulsed excitation into the $^4I_{13/2}$ at 1523 nm. The inset in (a) shows the temporal dependence of the $^4I_{11/2}$ emission upon excitation into the $^4I_{9/2}$ level at 825 nm. Lines are the results of fitting procedures (Vial's procedure (eq 1) or exponential decay, see text).

dx.doi.org/10.1021/cm4005745 | Chem. Mater. 2013, 25, 1912–1921

agreement with power dependence experiments (see Figure 4b). Both red $^4F_{9/2}$ and green $^4S_{3/2}$–$^2H_{11/2}$ UC emissions are governed by the long lifetime of the intermediate states. Further analysis of the temperature and concentration dependent dynamics of IR to NIR and VIS UC in Er^{3+}-doped Gd_2O_2S will be presented in another publication. We also measured for comparison the temporal evolution of the Er^{3+} UC luminescence from the $^4I_{11/2}$, $^4I_{9/2}$, $^4F_{9/2}$, and $^4S_{3/2}$–$^2H_{11/2}$ excited states in β-$NaYF_4$: 25%Er^{3+} after pulsed excitation into the $^4I_{13/2}$ at 1523 nm (Figure 8). Er^{3+} UC lifetimes are around five times longer in β-$NaYF_4$ than in Gd_2O_2S (see Figure 6), in agreement with the lower oscillator strength of Er^{3+} transitions in β-$NaYF_4$.

The time evolution of the UC emission intensities was fitted to an exponential decay or a Vial's type equation. The rise and decay times resulting from these fits are given in Table 3. The same trend as in Gd_2O_2S is observed for the $^4I_{11/2}$, $^4I_{9/2}$, and $^4F_{9/2}$ Er^{3+} UC emissions in β-$NaYF_4$: 25%Er^{3+} (Figure 8a, 8b and 8c). In particular, an immediate decay after the excitation pulse is detected for the $^4I_{9/2}$ UC luminescence, while an intensity rise before decaying is observed for both $^4I_{11/2}$ and $^4F_{9/2}$ UC emissions. Different to the behavior observed in Er^{3+}-doped Gd_2O_2S, only an immediate decay was detected for the green Er^{3+} UC emission from the $^4S_{3/2}$–$^2H_{11/2}$ excited state in β-$NaYF_4$. This observation suggests that the $^4I_{15/2} \rightarrow {}^4I_{13/2} \rightarrow {}^4I_{9/2} \rightarrow {}^4S_{3/2}$–$^2H_{11/2}$ GSA/ESA process is the dominant mechanism responsible for the $^4S_{3/2}$–$^2H_{11/2}$ population in Er^{3+}-doped β-$NaYF_4$. After a GSA/ESA process the emitting level is expected to decay with the intrinsic lifetime; however, the UC emission lifetime observed after excitation into the $^4I_{13/2}$ level is biexponential, with one component significantly longer than the intrinsic lifetime. This lengthening of the lifetime indicates that the ETU contribution to the UC mechanism populating the $^4S_{3/2}$–$^2H_{11/2}$ state is also important in Er^{3+}-doped β-$NaYF_4$.

CONCLUSIONS

Efficient IR to NIR UC luminescence has been demonstrated in Er^{3+}-doped Gd_2O_2S under monochromatic excitation at 1510 nm into the $^4I_{13/2}$ level of Er^{3+}. UC emission and quantum yield measurements show that Gd_2O_2S doped with 10% Er^{3+} (the optimum concentration) has an internal UC quantum yield of 12.0 ± 1.0% under 700 W/m^2 monochromatic excitation. Gd_2O_2S: Er^{3+} has a higher quantum yield for IR to NIR and VIS UC than the well-known Er^{3+}-doped β-$NaYF_4$ under monochromatic excitation, making it a promising UC material, also for photovoltaic applications. Time-resolved spectroscopy studies provide insight into the UC mechanism. ETU is the dominant mechanism for the IR to NIR UC luminescence, while both ETU and ESA contribute to the VIS green UC emission from the $^4S_{3/2}$ level.

AUTHOR INFORMATION

Corresponding Author

*E-mail: R.MartinRodriguez@uu.nl (R.M.-R.), A.Meijerink@uu.nl (A.M.).

Author Contributions

The manuscript was written through contributions of all authors. All authors have given approval to the final version of the manuscript.

Notes

The authors declare no competing financial interest.

ACKNOWLEDGMENTS

Financial support from the EU-FP7 NanoSpec programme (NMP-2009, grant agreement number 246200) is gratefully acknowledged.

ABBREVIATIONS

UC, upconversion; IR, infrared; c-Si, crystalline silicon; RE, rare-earth; NIR, near-infrared; VIS, visible; XRD, X-ray diffraction; SEM, scanning electron microscopy; OPO, optical parametric oscillator; PMT, photomultiplier; ETU, energy transfer upconversion; GSA, ground state absorption; ESA, excited state absorption

REFERENCES

(1) Sivakumar, S.; Diamente, P. R.; van Veggel, F. C. J. M. *Chem.—Eur. J.* **2006**, *12*, 5878.
(2) Nyk, M.; Kumar, R.; Ohulchanskyy, T. Y.; Bergey, E. J.; Prasad, P. N. *Nano Lett.* **2008**, *8*, 3834.
(3) Trupke, T.; Green, M. A.; Würfel, P. *J. Appl. Phys.* **2002**, *92*, 4117.
(4) Johnson, C. M.; Conibeer, G. J. *J. Appl. Phys.* **2012**, *112*, 103108.
(5) Shalav, A.; Richards, B. S.; Trupke, T.; Krämer, K. W.; Güdel, H. U. *Appl. Phys. Lett.* **2005**, *86*, 013505.
(6) Fischer, S.; Goldschmidt, J. C.; Löper, P.; Bauer, G. H.; Brüggemann, R.; Krämer, K. W.; Biner, D.; Hermle, M.; Glunz, S. W. *J. Appl. Phys.* **2010**, *108*, 044912.
(7) De Wild, J.; Rath, J. K.; Meijerink, A.; Van Sark, W.; Schropp, R. E. I. *Sol. Energy Mater. Sol. Cells* **2010**, *94*, 2395.
(8) Strümpel, C.; McCann, M.; Beaucarne, G.; Arkhipov, V.; Slaoui, A.; Svrcek, V.; del Cañizo, C.; Tobias, I. *Solar Energy Mater. Sol Cells* **2007**, *91*, 238.
(9) Wang, Y.; Ohwaki, J. *J. Appl. Phys.* **1993**, *74*, 1272.
(10) Lüthi, S. R.; Pollnau, M.; Güdel, H. U.; Hehlen, M. P. *Phys. Rev. B* **1999**, *60*, 162.
(11) Ivanova, S.; Pellé, F.; Tkachuk, A.; Joubert, M. F.; Guyot, Y.; Gapontzev, V. P. *J. Lumin.* **2008**, *128*, 914.
(12) Chen, G.; Ohulchanskyy, T. Y.; Kachynski, A.; Agren, H.; Prasad, P. N. *ACS Nano* **2011**, *5*, 4981.
(13) Kumar, G. A.; Pokhrel, M.; Sardar, D. K. *Mater. Lett.* **2012**, *68*, 395.
(14) Krämer, K. W.; Biner, D.; Frei, G.; Güdel, H. U.; Hehlen, M. P.; Lüthi, S. R. *Chem. Mater.* **2004**, *16*, 1244.
(15) Suyver, J. F.; Grimm, J.; van Veen, M. K.; Biner, D.; Krämer, K. W.; Güdel, H. U. *J. Lumin.* **2006**, *117*, 1.
(16) Renero-Lecuna, C.; Martín-Rodríguez, R.; Valiente, R.; González, J.; Rodríguez, F.; Krämer, K. W.; Güdel, H. U. *Chem. Mater.* **2011**, *23*, 3442.
(17) Eick, H. *J. Am. Chem. Soc.* **1958**, *80*, 43.
(18) Orlovskii, Y. V.; Basiev, T. T.; Pukhov, K. K.; Polyachenkova, M. V.; Fedorov, P. P.; Alimov, O. K.; Gorokhova, E. I.; Demidenko, V. A.; Khristich, O. A.; Zakalyukin, R. M. *J. Lumin.* **2007**, *125*, 201.
(19) van Schaik, W.; Blasse, G. *Chem. Mater.* **1992**, *4*, 410.
(20) Kumar, K.; Rai, S. B.; Rai, D. K. *J. Non-Cryst. Solids* **2007**, *353*, 1383.
(21) van Schaik, W.; Poort, S. H. M.; Schlotter, J. J. H.; Dorrestijn, E.; Blasse, G. *J. Electrochem. Soc.* **1994**, *141*, 2201.
(22) Auzel, F. *J. Lumin.* **1990**, *45*, 341.
(23) Pollnau, M.; Gamelin, D. R.; Lüthi, S. R.; Güdel, H. U.; Hehlen, M. P. *Phys. Rev. B* **2000**, *61*, 3337.
(24) MacDougall, S. K. W.; Ivaturi, A.; Marques-Hueso, J.; Krämer, K. W.; Richards, B. S. *Opt. Express* **2012**, *20*, A879.
(25) Jüstel, T.; Nikol, H.; Ronda, C. *Angew. Chem.* **1998**, *37*, 3084.
(26) Ebendorff-Heidepriem, H.; Ehrt, D.; Bettinelli, M.; Speghini, A. *SPIE Proceedings Rare-Earth-Doped Materials and Devices III*; SPIE: Bellingham, WA, 1999; Vol. *19*, p 3622.
(27) Buisson, R.; Vial, J. C. *J. Phys. (France) Lett.* **1981**, *42*, 115.
(28) Valiente, R.; Wenger, O. S.; Güdel, H. U. *J. Chem. Phys.* **2002**, *116*, 5196.